Int. J. Heat Mass Transfer. Vol. 36, No. 18, pp. 4397–4406, 1993
Printed in Great Britain

0017–9310/93 $6.00 + 0.00

An investigation on instantaneous local heat transfer coefficients in high-temperature fluidized beds—II. Statistical analysis

HONG-SHUN LI, REN-ZHANG QIAN,† WEN-DI HUANG and KAI-JUN BI
Department of Power Engineering, Huazhong University of Science and Technology, Wuhan, Hubei (Province) 430074, China

(*Received* 12 *November* 1992 *and in final form* 20 *May* 1993)

Abstract—Statistical analysis is employed to make a further insight into the nature of instantaneous local heat transfer coefficients obtained in Part I of this paper. The computed functions from these coefficients are the variance, autocorrelation function and power spectral density function. These functions and parameters have been employed to characterize the dynamic behaviors around the immersed horizontal tube and thus to investigate the mechanism of bed-to-tube heat transfer in high temperature fluidized beds. The bubble phase heat transfer component is separated from instantaneous local heat transfer coefficients, and is found to be increased approximately exponentially with increasing bed temperature.

INTRODUCTION

INSTANTANEOUS local heat transfer coefficients really reflect the heat transfer process between the bed and the immersed surface, and contain a great deal of important information to reveal the mechanism of this process. For example, the residence time of the particles or emulsion phase on the heat transfer surface, or the contact thermal resistance can be determined from the instantaneous local heat transfer coefficient or surface temperature [1–3]. Such data are imperative for validation or improvement of analytical models.

It is well known that the heat transfer between the bed and the immersed surface depends to a very large extent on the hydrodynamic behaviors of the bed and within the immediate vicinity of the immersed surface. In recent years, statistical analysis of the pressure fluctuations in fluidized beds has been employed to investigate the hydrodynamic behaviors of the beds [4, 5]. In a likewise manner the temperature fluctuation data of an immersed surface have been used to predict the hydrodynamic state by Saxena and Rao [6]. These investigations provided useful information concerning hydrodynamic characteristics of fluidized beds. However, none of the published works have been found in which instantaneous local heat transfer coefficients in high-temperature fluidized beds have been analyzed by using statistic theory related to the hydrodynamic behavior of the bed and around the immersed surface.

We have presented in Part I the time-average local heat transfer coefficients and spatial-average heat transfer coefficients in a fluidized bed with average temperature up to 1028°C. Here the instantaneous local heat transfer coefficients data are employed to investigate the fluidization behavior of the bed, the hydrodynamic conditions around the immersed horizontal tube and the mechanism of heat transfer process between the bed and the tube by statistic analysis method. The computed statistical functions are the variance, autocorrelation function and the power spectral density function.

ANALYSIS PROCEDURES

A brief description for the above-mentioned statistical functions which we plan to employ for the analysis and interpretation of instantaneous local heat transfer data is presented below.

For a time series which contains N instantaneous values, $x_1, x_2, \ldots, x_N$, obtained at equal time intervals Δt, the mean value μ of such N values is given as [7]:

$$\mu = \frac{1}{N}\sum_{i=1}^{N} x_i. \tag{1}$$

The scatter of data from this mean is referred to as the dispersion of data, and is described by the variance, σ, as:

$$\sigma^2 = \frac{1}{N-1}\sum_{i=1}^{N}(x_i-\mu)^2. \tag{2}$$

Here the division by $N-1$ gives an unbiased estimate of the variance. The positive square root of the variance σ is referred to as the standard deviation.

The autocorrelation function (acf) describes the general dependence of data at one moment on those at another moment, and is given by

† Address correspondence to Prof. Ren-Zhang Qian.

NOMENCLATURE

d_p	mean particle diameter
f	frequency
f_m	major frequency
h_{wb}	heat transfer coefficient between bubble phase and the immersed surface
h_θ	instantaneous local heat transfer coefficient at position θ
N	number of data points
$R_{xx}(\tau)$	autocorrelation function
r	lag number
$S_{xx}(f)$	power spectral density function
T_b	bed temperature
$T_{s\theta}$	instantaneous local surface temperature at angular position θ
$\bar{T}_{s\theta}$	time-average value of $T_{s\theta}$
u	gas velocity
x_i	ith value.

Greek symbols

Δt	time interval
θ	angular position on tube surface
μ	mean value
σ^2	variance
τ	time lag.

Subscript

θ	angular position on tube surface.

Abbreviations

acf	autocorrelation function
psdf	power spectral density function.

$$R_{xx}(r\Delta t) = \frac{1}{(N-r)\sigma^2} \sum_{i=1}^{N-r} (x_i-\mu)(x_{i+r}-\mu) \quad (3)$$

where r is referred to as the lag number. The number of possible products at each lag number, r, in equation (3) is only $N-r$, thus the division by $N-r$ gives an unbiased estimation of the autocorrelation function. Any deterministic data will have an autocorrelation function which persists over all time displacements, as opposed to random data which diminish to zero over large time displacements. A measured autocorrelation clearly provides a tool for detecting deterministic data which might be masked in a random background.

While the autocorrelation function expresses the behavior of the time series in the time domain, the power spectral density function (psdf), $S_{xx}(f)$, describes the behavior in the frequency domain. $S_{xx}(f)$ is the fourier transform of corresponding autocorrelation [7], i.e.

$$S_{xx}(f) = \sum_{r} R_{xx}(\tau)\cos(2\pi f\tau). \quad (4)$$

Here, the instantaneous local heat transfer coefficient data were filtered to eliminate any trend and then the stationary data set was employed to obtain power spectral density function through a Hamming window [7].

RESULTS AND DISCUSSIONS

Figure 1 shows 5 s of instantaneous local surface temperatures around the immersed horizontal tube for three angular positions at a mean bed temperature of 424 C and four different superficial gas velocities, the bed material is silica sand particles of 1.815 mm in mean diameter. These records are sampled at the recording speed of 125 Hz for a period of 30 s. The corresponding instantaneous local heat transfer coefficients are presented in Fig. 2. The computed autocorrelation functions, power spectral density functions and standard deviations for the instantaneous local heat transfer coefficients are given in Figs. 3–5, respectively. The reason why these experimental data are selected for presentation here is that the bed has changed from unfluidized state to well-fluidized state at this temperature with the variation of gas velocity, whereas the bed is well fluidized at other operating temperatures. The similar plots at $u = 2.09$ m s^{-1} are not shown for the sake of brevity since they resemble that at $u = 1.82$ m s^{-1}.

As shown in Figs. 1 and 2, the instantaneous local surface temperatures and heat transfer coefficients have experienced remarkable changes with the increase in gas velocity. The bed is not fluidized as the gas velocity is 1.26 m s^{-1}. It can be seen from Figs. 1(a) and 2(a) that $T_{s\theta}$ has little fluctuations in its value and, decreases gradually with time. This indicates the presence of an unfluidized stack of particles on the top of the tube. However, at the same time, the fluctuations of $T_{s\theta}$ and h_θ are fast, implying that local fluidization (or local bubbling) at the side of horizontal tube may occur though the bed is not fluidized. This phenomenon is consistent with the observation conducted in room temperature conditions [8]. From the corresponding psdf plot in Fig. 4(a), it is seen that the psdf contains many frequencies with a wide band and lower peak value. Moreover, the corresponding acf plot in Fig. 3(a), clearly shows that the fluctuation has more stochastic character. This can be established by the fact that the acf approaches to zero as the lag time is increased. These imply that the bubbles occur at the side of the tube with relatively strong randomness, and that the bubbles are small with various size in view of the fact that $h_{s\theta}$ fluctuates within a small range. However, the relatively lower time-average

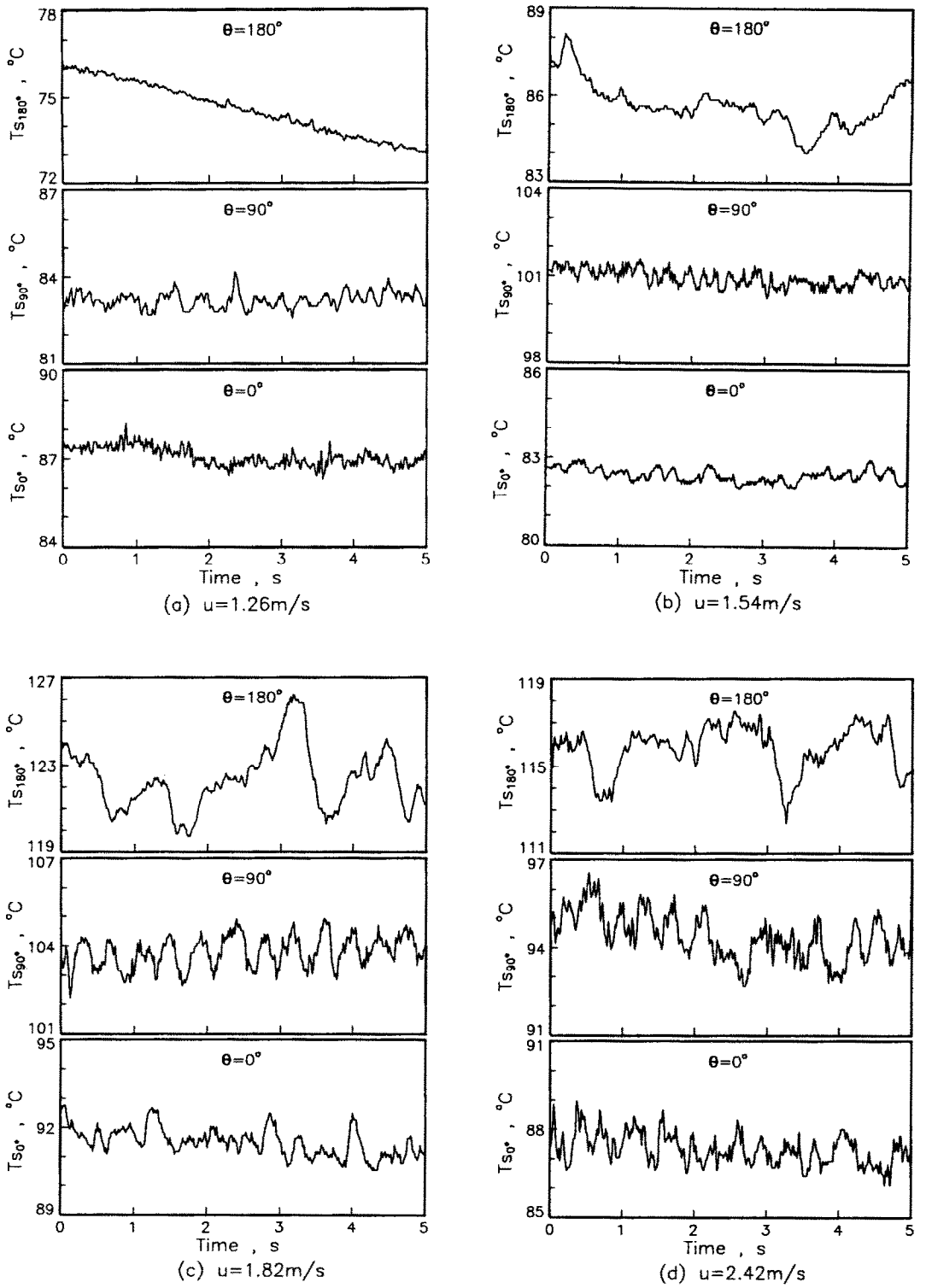

FIG. 1. Instantaneous local surface temperatures for $d_p = 1.815$ mm, $T_b = 424°C$.

value of h_{90} can be attributed to two possible sources. First, though at the side of the tube occurs local fluidization, the particles in the vicinity of this position move in a small range, new emulsion in bed bulk cannot move to here. Second, these small bubbles form into irregular chains of bubbles, resulting in a

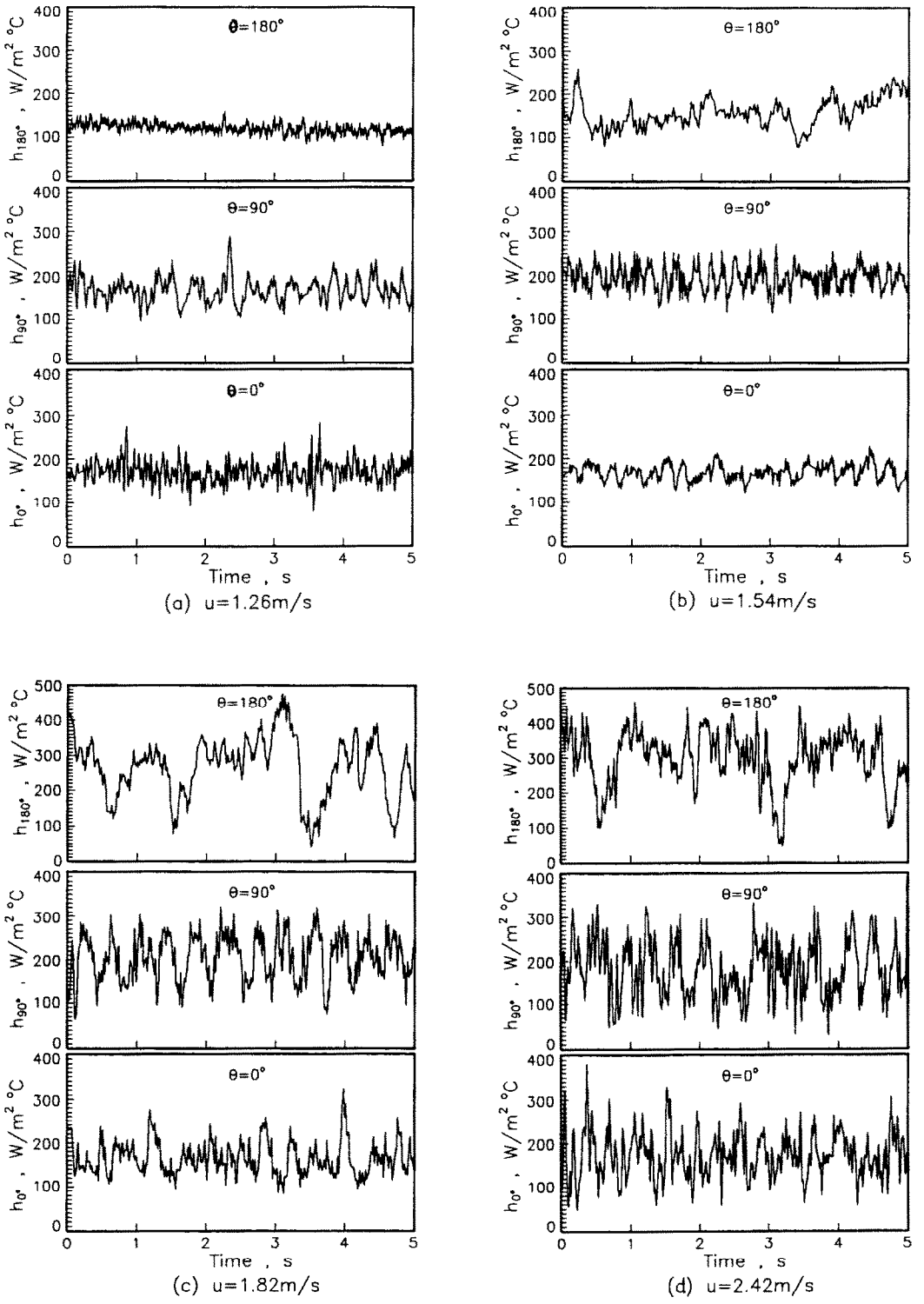

FIG. 2. Instantaneous local heat transfer coefficients for $d_p = 1.815$ mm, $T_b = 424$°C.

low time fraction of emulsion phase contact. At the same gas velocity, T_{S_0} and h_0 show the similar fluctuation pattern to that of $T_{S_{90}}$ and h_{90}, it can be conjectured that part of the bubbles at the side of the tube come from the gas film under the tube as observed at room temperature condition [8].

As the gas velocity increases to 1.54 m s^{-1}, the bed is fluidized. Fluctuation of $T_{S_{180}}$ in Fig. 1(b) and h_{180} in Fig. 2(b) appear. It is evident that the stack of defluidized particles, which remains on the top of the tube at lower gas velocity, is removed. However, the psdf plot of h_{180} in Fig. 4(b) shows that this movement

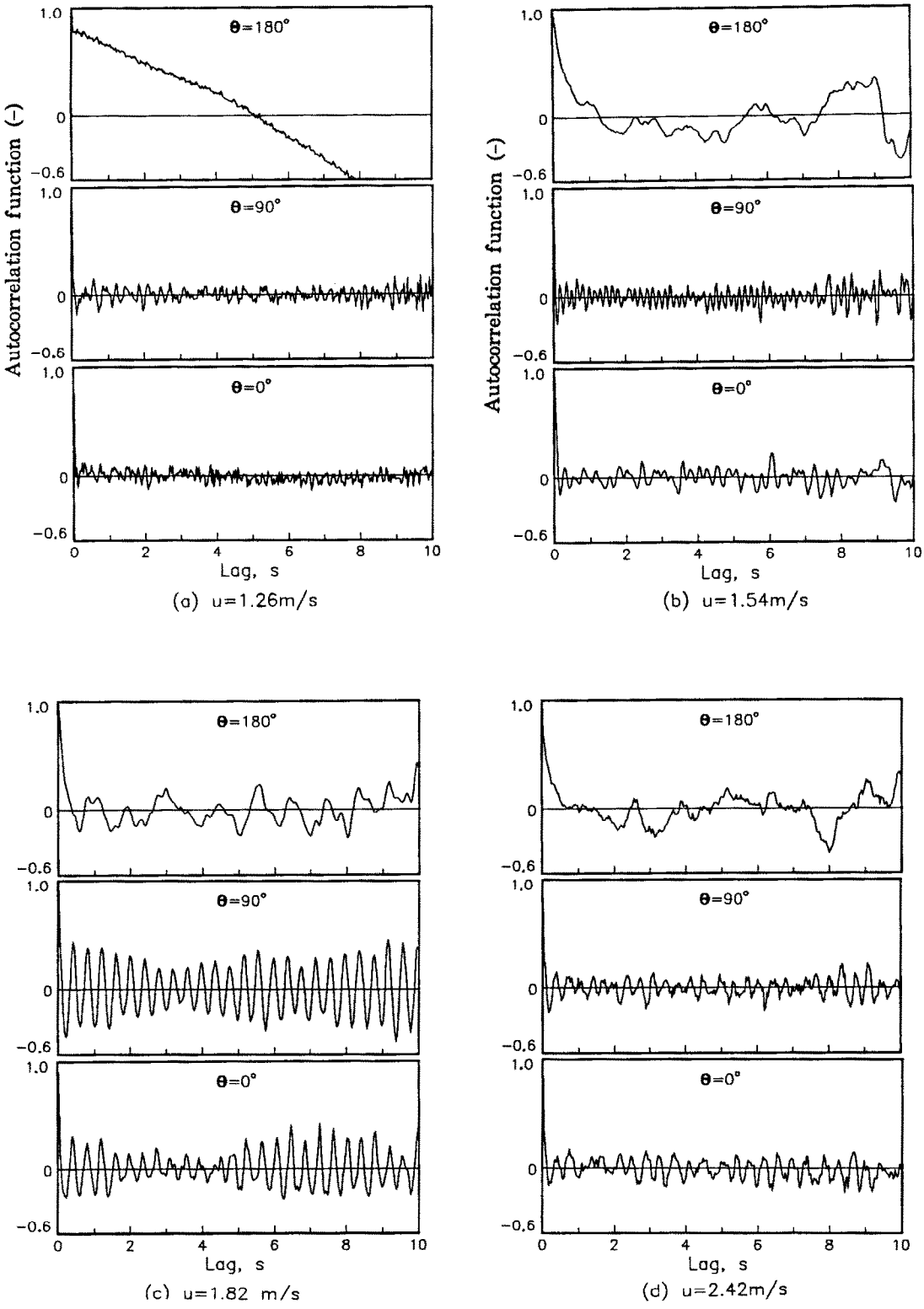

FIG. 3. Autocorrelation functions from instantaneous local heat transfer coefficient data for d_p = 1.815 mm, T_b = 424°C.

is slow. At this gas velocity, h_{90} exhibits a little stronger periodicity than at the gas velocity of 1.26 m s^{-1} and its psdf plot displays a somewhat narrower frequency band. This implies that the small bubbles have coalesced into a little larger bubbles, but the size range of these bubbles is still relatively larger.

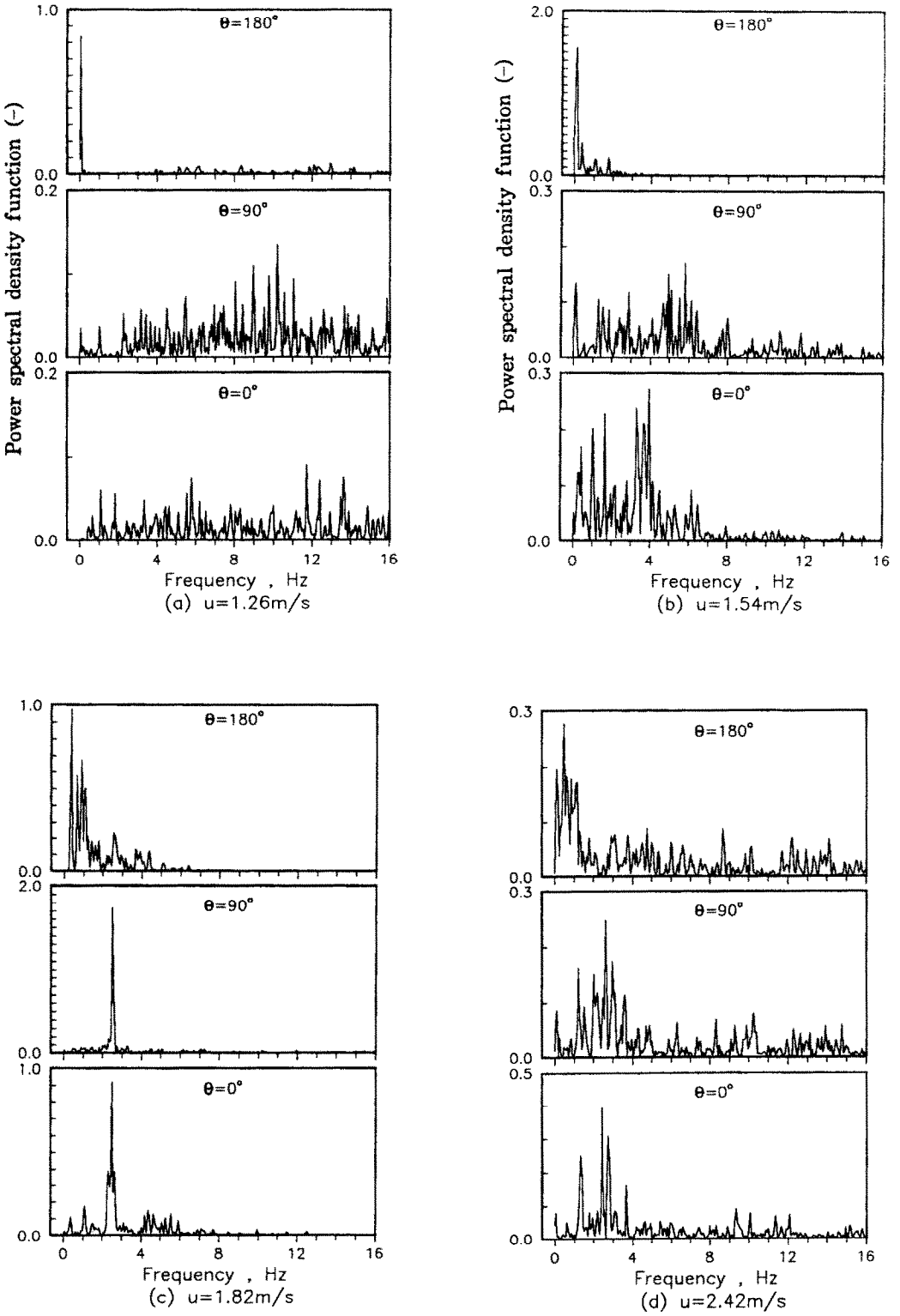

FIG. 4. Power spectral density functions from instantaneous local heat transfer coefficient data for d_p = 1.815 mm, T_h = 424°C.

When gas velocity increases to 1.82 m s^{-1}, T_{S_0}, $T_{S_{90}}$, h_0 and h_{90} in Figs. 1(c) and 2(c) exhibit periodic fluctuations, their acf plots in Fig. 3(c) indicate that their fluctuation signals are composed of strong deterministic component and little random component, also their psdf plots show that the fluctuation power

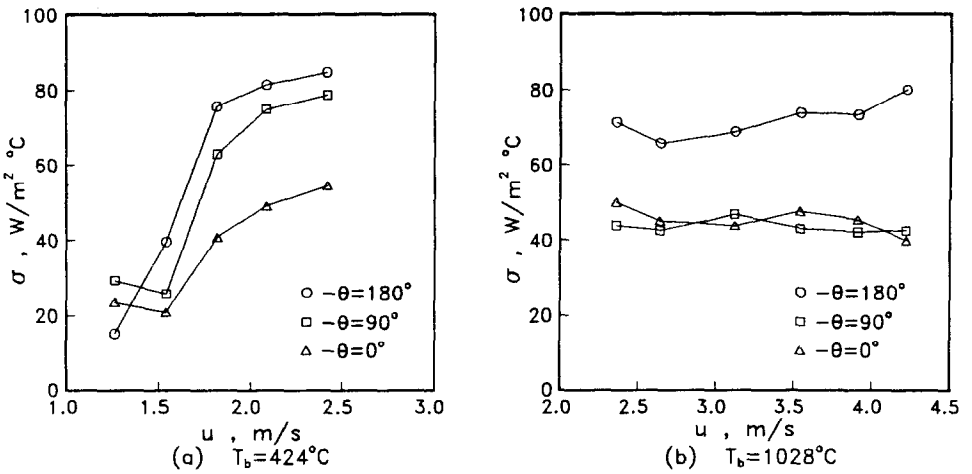

FIG. 5. Standard deviation in instantaneous local heat transfer coefficient data for d_p = 1.815 mm.

is almost concentrated on a single frequency. This implies a very narrow and stable bubble size distribution in the bed or the bed quality fluidization is very uniform. Also it can be seen that the fluctuation of h_{180} becomes faster. Moreover, the time-average value of h_{180} increases greatly, and becomes higher than that of h_{90} and h_0 (see Fig. 3(a) in Part I). At the gas velocity of 2.09 m s^{-1}, instantaneous local surface temperatures and heat transfer coefficients, and corresponding statistic functions are similar to that at 1.82 m s^{-1}, this suggests that the bed is at the same fluidization quality as at 1.82 m s^{-1}.

With further increase to 2.42 m s^{-1} in gas velocity, the fluidization state of the bed changes. The periodicities of the fluctuations of h_{90} and h_0 in Fig. 2(d) became a little weaker. This can be established by their acf plots in Fig. 3(d). Also the psdf plots of h_{90} and h_0 in Fig. 4(d) exhibit that the frequency bands become wider whereas the peak values become lower. This signifies that bubbles have disintegrated into smaller bubbles because the size of those bubbles has become larger than the maximum stable bubble size as a result of increment in gas velocity.

In each case of Fig. 4, it is clear that the signal power has a distinct maximum at a particular frequency. This dominant frequency is characterized here as the major frequency f_m and is representative of the most probable dense phase renewal frequency on the tube surface and hence the frequency of h_θ fluctuations. These major frequencies are listed in Table 1 as a function of gas velocity at mean bed temperature of 424°C. f_m is significantly different for different circumferential positions and gas velocities. At the gas velocity of 1.26 m s^{-1}, as above described, a stack of unfluidized particles exists on the top of the tube, thus the f_m of h_{180} is zero as expected. However, f_m for the 90° position and 0° position are above 10 Hz, implying a frequent renewal of particles and bubbles on the side and bottom of the tube. With increases in gas velocity, f_m for each angular position change in different ranges. f_m for the 180° position increases with increase in gas velocity. This, of course, is understandable on the basis of the fact that movement of particles on the top of the tube becomes more active with increase of gas velocity. On the other hand, f_m for the side and bottom of the tube initially increase rapidly as gas velocity is increased, but then the variations become insignificant. This suggests that the bubble frequency in the bed does not change significantly with further increases in gas velocity when the bed is well fluidized. However, the increase in gas velocity means increase in gas mass flow, thus it can be inferred that the volume of the bubbles increases, until it reaches the maximum stable bubble size.

f_m are listed in Table 2 for three angular positions and the same bed material at a mean bed temperature of 1028°C as a function of gas velocity. Under the operating conditions, as outlined in Part I of this paper, the bed is well fluidized. It is seen that f_m for the 180° position of the tube increases slowly with

Table 1. Major frequency for h_θ (d_p = 1.815 mm, T_b = 424 ± 14°C)

θ (deg)	f_m (Hz)				
	u = 1.26 m s^{-1}	u = 1.54 m s^{-1}	u = 1.82 m s^{-1}	u = 2.09 m s^{-1}	u = 2.42 m s^{-1}
180	0	0.183	0.366	0.610	0.549
90	10.376	5.671	2.502	2.686	2.625
0	11.597	3.967	2.502	2.502	2.441

Table 2. Major frequency for h_0 (d_p = 1.815 mm, T_b = 1028 ± 13 C)

θ (deg)	f_m (Hz) u = 2.36 m s^{-1}	u = 2.64 m s^{-1}	u = 3.12 m s^{-1}	u = 3.54 m s^{-1}	u = 3.91 m s^{-1}	u = 4.22 m s^{-1}
180	0.915	1.037	1.221	1.159	1.343	1.343
90	3.540	3.784	2.991	3.296	3.296	3.052
0	3.174	3.174	3.296	2.930	2.930	3.052

increase in gas velocity. On the other hand f_m for the 90° position and 0° position of the tube decrease slowly.

As described in Part I of this paper, with the increase in gas velocity, the time-average value of h_{180} initially increases rapidly, and then becomes much more than the time-average value of h_{90} and that of h_0. However, in the tables here, f_m for the 180° positions is much lower than f_m for the 90° position and 0° position. This phenomenon reveals that dynamic behavior on the top of the tube is different from that at other angular positions.

In Figs. 1 and 2, the characteristic of fluctuations of h_{180} is obviously different from that of h_{90} and h_0. For example, in Fig. 2(c) h_{90} exhibits a periodical fluctuation, whereas h_{180} has relatively random and slow fluctuation. Moreover, h_{180} often maintains at a relatively higher values for a relatively longer period of time, during which fluctuations of much higher frequency with smaller amplitude are observed. For example, see the time interval 1.9–3.2 s in Fig. 2(c). Then this period is followed by a rapid decrease with much shorter time interval. Even where there is a stack of unfluidized particles on the top of the tube at lower gas velocity, as shown in Fig. 2(a), no such rapid decrease is observed. Thus it can be deduced that the aforementioned rapid decrease is caused by a void which emerges on the top of the tube. It is improbable that bubbles in the bed may move to the rear of the tube and contact with the top surface of the tube. Thus this void may be caused by the fast moving away of the particles on the top of the tube, but the movement of those particles is caused by passing bubbles. However, this void rapidly disappears because of the filling of new particles. The above mentioned period of relatively longer time during which higher h_{180} is observed, can be attributed to the fact that the particles on the top of the tube slide to the side of the tube along the direction of circumference, while new particles continually replenish onto the top of the tube, as shown in Fig. 6. During this sliding process, the void may appear on the rear of the tube due to the possible intense disturbance of passing bubbles. On the other hand, the side of the tube contacts alternatively with dense phase and bubble phase. Thus the time fraction of local dense phase contact on the top of the tube is much higher than at the side of the tube.

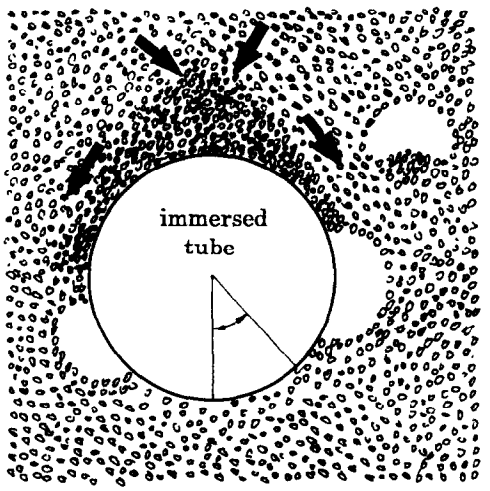

FIG. 6. Dynamic behavior around the horizontal immersed tube.

As seen in Fig. 2, the wave crest values of fluctuations of h_{180} are much higher than that of h_{90} and h_0. This phenomenon is more pronounced at higher bed temperatures, for example, see Fig. 2 in Part I of this paper. This can be attributed to two sources. First, the voidage of sense phase on the top of the tube is smaller than that at the side and bottom of the tube. Second, particles contact more closely with the top surface of the tube than with the side and bottom surface because of the action of gravity. Thus the gas film thickness is very thin, which in turn results in higher local heat transfer coefficient for the top of the tube.

Because of the above described facts that the top surface of the tube has a higher time fraction of dense phase contact, and experiences much higher heat transfer coefficient during periods of local dense phase contact than that at the side of the tube at higher gas velocity, therefore, the time-average values of h_{180} are much higher than that of h_{90}, this is just the phenomenon observed in Part I of this paper.

As the bed is not fluidized, the movement of particles on the top of the tube is feeble. With increase in gas velocity, this movement becomes more active, but further increase in gas velocity results in much more movement of the particles, which in turn may result in more voids on the top of the tube, thus the time fraction of the dense phase contact on the top of the tube decrease with further increase in gas velocity. This is why the time-average values of h_{180} initially increase as gas velocity is increased, but then decreases

as gas velocity is increased further, which is observed in Part I of this paper. In Part I, it is also observed that the time-average value of h_{90} decreases as gas velocity is increased when the bed is well fluidized. This is obviously due to the fact that the time fraction of bubble phase contact at the side of the tube increases with increase in gas velocity. But this decrease becomes more gradual at higher bed temperatures, this can be attributed to the contribution of radiant heat transfer which increases monotonously with increase in bed temperature. On the other hand, h_0 approximately increases monotonicaly, but slowly, with increase in gas velocity. This can be attributed to the fact that the bed voidage within the vicinity of the bottom of the tube is relatively larger at lower gas velocities. With increase in gas velocity, the particle population becomes larger and larger, thus the time fraction of particles contact at the bottom of the tube becomes higher and higher, and the bottom experience renewal type of contact with dense phase contribution becoming important, as shown in Figs. 2(b) and (c). This observation is consistent with those conducted at room temperature condition [9].

Figure 5(a) shows the computed standard deviations for instantaneous local heat transfer coefficients in Fig. 2. It is seen that σ for h_{180} initially increases rapidly as gas velocity is increased, but then the increase becomes much more gradual as gas velocity increases further. On the other hand, both the σ plots of h_{90} and h_0 exhibit a minimum at the gas velocity of 1.54 m s^{-1}, thereafter they exhibit the same variation features as observed above for the σ of h_{180}.

As aforementioned, with increase in gas velocity, the movement of the particles on the top of the tube become more and more violent. Therefore, the range of h_{180} fluctuation becomes larger and larger, this results in continuous increase of σ of h_{180} with increasing gas velocity. At the gas velocity of 1.54 m s^{-1}, the bed is just fluidized, but why is the σ value of h_{80} smaller instead of larger at this gas velocity than at 1.26 m s^{-1}? As already indicated, though the bed is not fluidized at the gas velocity of 1.26 m s^{-1} many small bubbles form into irregular chains of bubbles around the side of the tube, which results in relatively longer residence time of bubble phase, which in turn produces relatively larger magnitude of fluctuations of h_{90}. This will cause the standard deviation to increase. As the gas velocity increases to 1.54 m s^{-1}, small bubbles coalesce into a little larger bubbles, the latter move faster than the former, therefore it is not very probable that chains of bubbles will form on the windward side of the tube. However, overall, those coalesced bubbles are still small, thus the magnitude of fluctuation of h_{90} is smaller instead of larger at this stage than at 1.26 m s^{-1}. In room temperature fluidized beds, Saxena and Rao [10] also observed that the σ plot of instantaneous local surface temperature fluctuation at $\theta = 60^\circ$ position on a horizontal immersed tube exhibits a minimum value as the gas velocity is a little beyond the minimum fluidizing gas velocity, but those investigators did not give the reasons for this phenomenon.

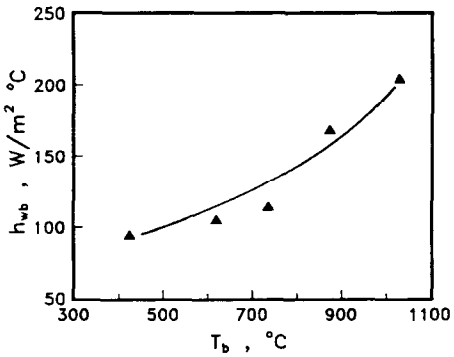

FIG. 7. Variation of h_{wb} with bed temperature.

In Fig. 5(a), both the σ plots for h_{90} and h_0 at $T_b = 424$°C increase rapidly as gas velocity increases from 1.54 to 1.82 m s^{-1}, this is suggestive of a rapid increase in bubble size with increase in gas velocity. However, with further increase in gas velocity, the aforementioned increase slows down. This implies that further increase in gas velocity does not produce large changes in bubble size. Obviously, the bubbles' behavior as revealed here is consistent with the conclusions drawn earlier on the basis of acf and psdf plots of instantaneous local heat transfer coefficients. In Fig. 5(b), the values of σ are shown as a function of gas velocity for the same bed material at mean bed temperature of 1028°C, for which the bed is well fluidized. However, the value of σ for h_{180} increases slowly with increase in gas velocity, whereas values of σ for h_{90} and h_0 do not exhibit any appreciable change with increase in gas velocity. This indicates that a stable bubble size distribution exists in the bed and there is an equilibrium between the bubble growth and breakup.

To sum up, the variance, or standard deviation, in instantaneous local heat transfer coefficient fluctuation data exhibits a characteristic variation with increase in gas velocity, thus it may be employed to characterize the bed hydrodynamics and dynamic behavior around the immersed tube.

An interesting observation can be made from inspection of Figs. 2(c) and (d) and Fig. 2 in Part I. h_{90} plots in Figs. 2(c) and (d) display the lowest values of about 100 W m^{-2} °C^{-1}, whereas the similar result in Fig. 2 in Part I is about 200 W m^{-2} °C^{-1}. As conjectured earlier, the lower heat transfer coefficients are interpreted to be periods of local bubble phase contact with the surface of the tube. Figure 7 shows values of h_{wb}, the heat transfer coefficient between bubble phase and surface of the tube, as a function of bed temperature, these values are obtained by the following method: the ten lowest values are selected at each of ten neighboring troughs in fluctuation of h_{90} under the operating condition of mean bed tem-

perature of 424°C and gas velocity of 2.09 m s^{-1}, then h_{wb} is obtained from the arithmetic mean of these lowest values. The same step is repeated for operating conditions 618°C and 2.48 m s^{-1}, 735°C and 2.40 m s^{-1}, 872°C and 2.44 m s^{-1}, 1028°C and 2.36 m s^{-1}, thus values of h_{wb} for all the operating bed temperatures are obtained. It is seen that h_{wb} approximately increases exponentially with increase in bed temperature. This can be attributed to the contribution of radiant heat transfer which increases rapidly with increase in bed temperature because of the large value of $(T_b^4 - T_{s_{in}}^4)$. No such observation for high temperature operating conditions has been reported in the literature till now, and therefore, the variation of h_{wb} with bed temperature here cannot be compared directly with other investigations.

During periods of local bubble phase contact, it is observed that instantaneous local heat transfer coefficients exhibit high frequency yet small magnitude fluctuations. This could be due to the facts that turbulent flow exists in the boundary layer during periods of bubble phase contact, and that a small number of particles exists in bubble phase.

CONCLUSIONS

On the basis of the above investigations, several conclusions can be drawn as follows.

(a) Local dynamic behaviors around a horizontal tube immersed in a high temperature fluidized bed are found to be significantly different for different circumferential positions and gas velocities. At lower gas velocities, a relatively cool defluidized stack of particles exists on the top of the tube. With increase in gas velocity, the movement of particles on the top of the tube become faster. This gradually results in a continued particle flow. Thus the local heat transfer coefficient increases rapidly. With further increase in gas velocity, more and more voids emerge on this position as a result of disturbance of passing bubbles. This in turn results in the increase in time fraction of bubble phase contact. Thus the time-average values of h_{180} will decrease gradually. On the other hand, the side of the tube is alternatively contacted with the bubble phase and emulsion phase. As for the bottom of the tube, at lower gas velocity, it has lower particle population, with increase in gas velocity, more and more particles per unit time impact onto the bottom portion of the tube, and eventually, this angular position experiences renewal type of contact with dense phase and bubble phase. Thus, the time-average value of h_0 increases approximately monotonously with increase in gas velocity.

(b) As the bed is not fluidized, local fluidization may occur at the side of the tube. At the same time many small bubbles may form into chains of bubbles around this angular position. But the emergence and movement of those small bubbles have much more stochastic character. With increase in gas velocity, those small bubbles will coalesce into larger bubbles. At this stage, the alternate contacts of bubble phase and dense phase with the windward side of the tube exhibit a good periodicity. However, as the size of bubbles becomes beyond the maximum stable bubble size, they will break up into smaller bubbles, then the aforementioned alternate contacts exhibit more stochastic character.

(c) h_{wb} approximately increases exponentially with increase in bed temperature.

Acknowledgement The authors wish to express their sincere thanks to Professor B. X. Wang of Tsinghua University for refining on the English manuscripts.

REFERENCES

1. H. S. Mickley, D. F. Fairbanks and R. D. Hawthorn, The relation between the transfer coefficient and thermal fluctuations in fluidized-bed heat transfer. *Chem. Engng Prog. Symp. Ser.* **57**(32), 51–60 (1961).
2. H. S. Zhang, G. Q. Huang and C. L. Xie, The heat transfer model and experimental study of single horizontal tube immersed in the fluidized bed combustion boiler (in Chinese), *J. Engng Thermophys.* (China) **4**, 53–60 (1983).
3. A. P. Baskakov, B. V. Berg, O. K. Vitt, N. F. Filippovsky, V. A. Kirakosyan, J. M. Goldobin and V. K. Majkaev, Heat transfer to objects immersed in fluidized beds, *Power Technol.* **8**, 273–278 (1973).
4. L. T. Fan, Y. W. Huang, D. Neogi and N. Utani, Statistical analysis of temperature effects on pressure fluctuations in a gas solid fluidized bed, *Fluidization '85. Science and Technology. Proc. of the Second China Japan Symposium*, Kumming, China. Science Press, Beijing (1985).
5. S. C. Saxena and N. S. Rao, Pressure fluctuations in a gas fluidized bed and fluidizations quality, *Energy* **15**, 489–497 (1990).
6. S. C. Saxena and N. S. Rao, Fluidization characteristics of gas-fluidized beds: air and glass beads system, *Energy* **14**, 811–826 (1989).
7. W. Q. Yang and L. Gu, *Time Series Analysis and Modeling of Dynamic Data* (2nd Edn, in Chinese). Beijing Institute of Technology Press, Beijing (1988).
8. D. Harrison and J. R. Grace, Fluidized beds with internal battles. In *Fluidization* (Edited by J. F. Davidson and D. Harrison), pp. 599–626. Academic Press, London (1971).
9. R. Chandran and J. C. Chen, Bed-surface contact dynamics for horizontal tubes in fluidized beds, *A.I.Ch.E. Jl* **28**, 907–914 (1990).
10. S. C. Saxena and N. S. Rao, Determination of fluidization quality of beds of spherical particles. *Energy* **16**, 1199–1206 (1991).